J. Fluid Mech. (1978), *vol.* 86, *part* 2, *pp.* 313–335
Printed in Great Britain

An experimental map of the internal structure of a vortex breakdown

By J. H. FALER† AND S. LEIBOVICH

Sibley School of Mechanical and Aerospace Engineering, Upson Hall, Cornell University, Ithaca, New York 14853

(Received 24 January 1977 and in revised form 1 August 1977)

The flow field of an 'axisymmetric' vortex breakdown has been mapped using a laser-Doppler anemometer. The interior of the recirculation zone is dominated by energetic, non-axisymmetric, low frequency periodic fluctuations. Spectra for a number of points inside this zone, as well as time-averaged swirl and axial velocity profiles both inside and outside the recirculation zone, have been obtained. The time-averaged streamlines in the interior show an unexpected two-celled structure attributed to the action of the fluctuations. Although the present experiment deals with one particular breakdown, flow-visualization studies indicate that the case examined is typical of the 'axisymmetric' form of breakdown over a range of flow conditions.

1. Introduction

By the term 'vortex breakdown', we mean the abrupt occurrence of an internal stagnation point on the axis of a concentrated vortex with an axial flow. Vortex breakdown was first identified by Peckham & Atkinson (1957) in leading-edge vortices formed above wings with highly swept leading edges and was studied extensively because of its potential importance in aerodynamics (e.g. Elle 1958; Lambourne & Bryer 1961; Hummel 1965).

In order to isolate the phenomenon in more controlled circumstances, experiments on vortices confined in tubes were devised shortly thereafter by Harvey (1962) and Kirkpatrick (1964). The principal problem formulated by theorists was to discover the conditions which would lead to the 'breakdown' of a vortex, and the theories of Squire (1962), Benjamin (1962, 1967), Gartshore (1962), Hall (1967), Ludwieg (1961, 1962), Mager (1972) and others address this problem: this work is reviewed by Hall (1972).

Vortex breakdown, however, arises in technological contexts other than aerodynamics, and the important questions, from a technological point of view, may go beyond the need to predict what kind of vortices will suffer breakdown. One significant example is the deliberate production of flows of the vortex-breakdown family in combustion chambers to produce a recirculation region that serves as a fluid-dynamic flame holder. Other technological applications have been discussed by Sarpkaya (1971*b*) and by Cassidy (1969).

A theory limited to predicting whether or not a given vortex will break down is

† Present address: Corning Glass Works, Corning, New York.

insufficient in applications such as combustors. A much more complete treatment is needed to describe the major features of the recirculation zone itself. Some theories (Bossel 1969; Leibovich 1968, 1970; Leibovich & Randall 1973; Randall & Leibovich 1973) and numerical experiments with the Navier–Stokes equations by Kopecky & Torrance (1973) and by Grabowski & Berger (1976) address this question; but, as Leibovich (1978) has pointed out, none of the existing treatments seem adequately to predict flow fields observed in 'real' breakdowns.

One difficulty faced by theoreticians is the lack of detailed information concerning flows following vortex breakdown. Although experiments done by Kirkpatrick (1964), Sarpkaya (1971*a*, *b*) and others previously mentioned have produced much useful information (mainly by flow visualization) none provide velocity data in the interior of the recirculation zone. Conventional velocity probes can significantly alter highly responsive swirling flows, and their use is therefore precluded.

Large amplitude disruptions of concentrated vortex cores take place under a wide variety of flow conditions and take numerous forms, including the 'axisymmetric' and spiral forms of vortex breakdown described as early as 1961 by Lambourne & Bryer, and the spectacular double-helix first reported by Sarpkaya (1971*a*, *b*). These are among six distinct disturbance modes reported by Faler & Leibovich (1977, henceforth abbreviated as FL).

In this paper the regions inside and surrounding the recirculation zone of an axisymmetric (or 'bubble-like') breakdown (plate 1) in water are mapped using a laser-Doppler anemometer. The apparatus is similar in design to Sarpkaya's (1971*a*).

As has been already observed by Sarpkaya (1971*a*, *b*), the internal flow in the bubble form of vortex breakdown is neither axisymmetric nor steady, but is dominated by vigorous low frequency periodic fluctuations in time and azimuth. This we confirm by visual observations and by power spectra of the velocity fields at a number of points within the recirculation zone. We also construct from time-averaged velocity data (under the assumption that the time-averaged motion is axisymmetric) the time-averaged stream function in and around the recirculation zone. The most interesting feature of the mean streamlines is a two-celled structure of the recirculation zone; in addition to the two stagnation points marking the beginning and end of the recirculation zone, there are two other internal stagnation points on the axis.

A brief survey of features of vortex breakdowns and their connexion with related disruptions of vortex cores is given in § 2 as a contextual aid. Additional experiments in the present apparatus, to be reported elsewhere by Garg & Leibovich (1978), show that qualitative features of axisymmetric and spiral vortex breakdowns seen in the present series of experiments at Reynolds numbers up to 8000 remain unaltered up to Reynolds numbers of 21 000. Thus, although the present data are for a moderate Reynolds number (2560), the results are probably generic.

2. Résumé of qualitative observations

The purpose of this section is to place the present results in context by briefly summarizing some relevant visual information gathered for a range of flow conditions.

Many features to be described have been reported previously, and the papers by Sarpkaya (1971*a*, *b*, 1974) are the most immediately relevant. We shall outline the

findings of Faler & Leibovich (1977) since, for the present discussion, they are more extensive and (more important) were observed in the same apparatus.

If the volume rate of flow is held fixed and the swirl slowly and steadily increased from low values, a sequence of very large amplitude azimuthally asymmetric disturbances is seen. These include Sarpkaya's (1971*a*, *b*) double helix and five other distinctive disturbance forms described in some detail in FL. Of the six disturbance forms (a seventh mode, called type 1 by FL, is a variant of the so-called 'axisymmetric', or type 0, vortex breakdown) four are associated with an internal stagnation point, and therefore fall into the category that we identify as vortex breakdown. Of these four, two are the (by now classic) 'axisymmetric' ('bubble') and 'spiral' forms of vortex breakdown. For sufficiently high Reynolds numbers, only these latter forms of vortex breakdown are observed to occur in our apparatus.

The disturbances observed follow a definite order of progression as the swirl is increased, and there is therefore a clear evolutionary pattern. *All* disturbances in this hierarchy, including the bubble form of vortex breakdown, are very obviously asymmetric in azimuth.

While there is a definite progression of forms, there are numerous borderline ranges of flow settings for which the disturbances change to neighbouring forms apparently spontaneously (or at least with no prompting). This is connected with what Sarpkaya (1971*a*, *b*) described as 'hysteresis' effects, but we found no true hysteresis phenomena in our experiments.

In the progression of forms as the swirl is increased, spiral breakdowns *always* occurred before axisymmetric breakdowns, which were always the final forms in the progression.

Both spiral and axisymmetric vortex breakdowns show high degrees of structural stability, except for flow settings permitting spontaneous transformations between types. On the other hand, they exhibit a considerable amount of positional instability; breakdowns tend to wander back and forth on the axis in an unpredictable way with no noticeable change in external conditions. These wanderings occur within specific limits about a mean position. The mean position of the spiral breakdown at any given Reynolds number is always well downstream of the mean position of the axisymmetric breakdown.

The interior motion of the axisymmetric breakdown is visually both unsteady and asymmetric in azimuth, as clearly described by Sarpkaya (1971*a*). Fluid is injected into and ejected out of the interior by an emptying and filling process at the rear of the breakdown.

These brief descriptions of events occurring when the external conditions of the experiment are held fixed are sufficient to set the stage for the detailed velocity map to be reported in this paper. Interesting transient motions change the visual appearance of the disturbances, but these effects are not of interest here. Further information on transients, and a more exhaustive description of events, may be found in Sarpkaya's (1971*a*, *b*, 1974) papers, and in FL.

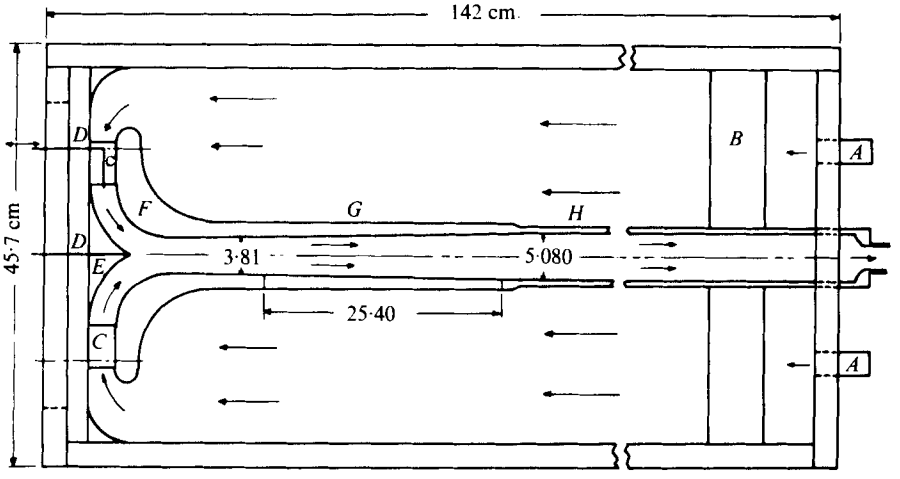

FIGURE 2. Test tank layout and dimensions. *A*, inlet pipes (2 of 6 shown); *B*, foam baffle; *C*, swirl vanes (2 of 32 shown); *D*, dye injector tubes; *E*, centre-body; *F*, entrance channel bell-mouth; *G*, test section; *H*, exit pipe.

3. Experimental apparatus

Flow apparatus

The flow apparatus, which consisted of upper and lower constant-head tanks, a test tank, a rotameter, and the necessary piping, valves and filters, was similar to that used by Sarpkaya (1971*a*, *b*). It is described in more detail by FL, and in great detail by Faler (1976). Water was supplied to the test tank (figure 2) from the upper constant-head tank and left the tank through an exit pipe, a precision rotameter and a large needle valve, then entering the lower constant-head tank. A plate bolted to one end wall of the tank supported 32 guide vanes, a planetary gear system to control the vane orientation, and a Plexiglas centre-body to direct the flow into the test section. The desired swirl was imparted to the fluid by the vanes. The planetary gear system rotated all the vanes in unison; at any setting, each vane made the same angle with a radial line drawn from the centre of the brass plate to the pivot line of the vane. This angle could be varied continuously from 0 to 60°.

Water was directed through the vane array by an annular channel formed on one side by the brass plate and attached centre-body and on the other by a bell-shaped piece, also made of Plexiglas. The test section, machined from Plexiglas and highly polished, was joined upstream to the bell-shaped piece and downstream to a constant-diameter Plexiglas exit pipe.

A straight-walled section, 3·81 cm in diameter and 10·5 cm long, followed the contraction formed by the bellmouth. Downstream of this straight section, the inside diameter of the test section increased linearly from 3·81 cm to 5·08 cm in an axial distance of 25·4 cm (tube-wall divergence angle of 1·43°). The diverging section was followed by another constant-area section, of diameter 5·08 cm, which extended beyond the tank end wall; the area was then smoothly reduced to an inside diameter of 2·54 cm.

Dye could be introduced into the flow at two locations. One dye injector was a piece of hypodermic tubing along the centre-line of the Plexiglas centre-body and pro-

truding slightly into the fluid. This provided a marker filament along the tube axis. The second injector, installed into one specially modified guide vane, allowed dye to be introduced at various radial locations in the tube.

Adjustable parameters

The parameters that could be systematically varied and monitored were the volume flow rate and vane angle, described by the Reynolds number Re and the circulation number Ω.

The Reynolds number used was based on the average (based upon flow rate) axial velocity $\overline{W}$ and the diameter D of the test section at the throat, before the divergence. The dimensionless circulation number Ω was defined by

$$\Omega \equiv \Gamma / \overline{W} D,$$

where $\Gamma = 2\pi R_{te} V$ is the circulation at the trailing edge of the swirl vane; R_{te} is the radial distance from the tube centre to the trailing edge of the vanes and V is the azimuthal velocity of the fluid leaving the vanes. A physical interpretation of Ω may be visualized by assuming inviscid steady flow: then the circulation is constant on stream surfaces and, in particular, Γ is constant at the tube wall, therefore Ω is an estimate of the ratio of the swirl velocity at the wall to the average axial velocity in the tube.

Instrumentation

Since previous investigators (e.g. Kirkpatrick 1964; Hummel 1965) have reported that vortex-breakdown flows were significantly disturbed by conventional velocity measuring methods, velocity measurements were taken with a DISA type 55L laser-Doppler anemometer system using the dual-scatter mode of operation. The DISA optical frequency shift unit, comprised of two Bragg cells driven at different frequencies, was used during the later stages of the study; this device improved the tracking ability of the signal processor and permitted the resolution of low and reversed velocities.

The optical components were mounted on traversing devices which permitted accurate initial alignment and precise movement in the axial and radial directions. The optical arrangement permitted radial traverses in a meridional plane from just inside the tube wall to a point slightly beyond the tube centre-line: the axial symmetry of the velocity profile could therefore be checked only near the tube centre-line.

Refraction from the various optical interfaces and the tapered flow duct of circular cross-section were taken into account when determining the size of the beam intersection volume, the local beam intersection angle, and the relationship between the optical component position and the location of the beam intersection in the flow. The spatial resolution of the device, determined by the size and orientation of the intersection volume, was improved by fitting a 3 × beam expander on the laser head and by using a lens of the shortest focal length compatible with the optical system and flow device set-up. The intersection volume was approximately cylindrical, with diameter equal to 0·08 mm and length equal to 0·43 mm, and the axis of the cylinder was oriented radially.

The output from the signal processor was measured using a digital voltmeter to

determine the mean velocity. After low-pass filtering and d.c. suppression, the analog signal was recorded on a strip chart; velocity fluctuations were determined from this record or from an r.m.s. voltmeter. Detailed descriptions of the instrumentation, alignment procedures, and laser beam paths through the flow device are given in Faler (1976).

Since some of our measurements were made with and some without the frequency shift unit, and with different procedures depending upon which part of the flow was being treated, a discussion of errors would be somewhat lengthy. Instead, a list is given of the maximum estimated errors for signals that could be stably tracked: for data upstream of the breakdown, the maximum errors are expected to be $\pm 0{\cdot}4$ cm/s; for time-averaged data in and downstream of the breakdown, the maximum errors are expected to be $\pm 0{\cdot}24$ cm/s; and for instantaneous data in and downstream of the breakdown, the errors are $\pm 0{\cdot}38$ cm/s. For most measurements, the anticipated errors are significantly smaller than those indicated, and a more complete discussion of the errors in any given data set is given in Faler (1976). For regions of the flow involving large radial velocity gradients, difficulty was sometimes encountered in tracking the signal, and under these conditions, reproducibility was poor and some scatter occurs in the data.

4. Experimental procedure

As described in § 2, vortex breakdowns tend to wander back and forth along the tube axis despite the precautions taken to ensure steady flow conditions. Furthermore, portions of the interior of the recirculation zone (which we abbreviate as RZ henceforth; we also call this region the 'bubble') are dominated by low frequency velocity fluctuations with peak-to-peak amplitudes that can exceed mean values. These facts, taken together, present obvious experimental problems when measurements are made inside the RZ. We therefore sought flow conditions that produced an axisymmetric breakdown with minimal positional excursions. The flow with $Re = 2560$ and $\Omega = 1{\cdot}777$ seemed the most suitable; it produced a breakdown that remained stationary for long periods of time, and axial excursions were no more than 7 mm.

Visual observations indicated that vortex-breakdown flows have a remarkable structural integrity. Provided that the axial location of the breakdown did not vary greatly, this suggests that the velocity fields in the neighbourhood of a breakdown RZ depend upon the position relative to a fixed point of the breakdown structure, such as the front stagnation point, and not on the absolute axial location. Measurements confirmed this, and our procedure, described below, depends upon this fact.

A magnifying lens and mirror were mounted on top of the flow apparatus and adjusted to eliminate parallax; when properly placed, an observer could view the nose region of the bubble as it drifted axially. A transparent scale on the top outside surface of the test section allowed the axial position of the nose of the breakdown to be determined with a precision of better than 0·5 mm.

For each radial position of the laser probe volume the velocity was continuously measured by the frequency tracker and the position of the breakdown nose was monitored by sighting through the viewing system. As the breakdown wandered axially, it occasionally rested in one axial position for a period of time (typically several seconds). When this occurred, the voltmeter output was held fixed by means of

a remote switch. The voltage reading and the position of the probe volume and bubble nose were then recorded. Several velocity readings were taken for each measuring-point position and relative breakdown position. Readings obtained in this manner were repeatable, even for positions for which spatial variations of the velocity were considerable (e.g. just upstream of the bubble nose and near the tube centre-line). In nearly all cases the standard deviation of the velocity readings (with the measuring point and relative breakdown position fixed) was less than about 4 % of the mean of the readings. In no case were data at a given radial location taken when the axial location of the breakdown shifted by more than 3 mm. By repeating this procedure at various axial and radial locations it was possible to build, bit by bit, a detailed velocity map of the flow outside the bubble envelope.

In regions where the velocity fluctuations as well as the mean velocity were of interest (e.g. inside the bubble and in the wake region) a slightly different procedure was used. The analog voltage output was low-pass filtered (using a 10 Hz cut-off) and then suppressed with a known d.c. voltage. This conditioning allowed the signal to be recorded on one channel of a strip-chart recorder which was set at a fairly high sensitivity.

A second channel was used at times to record the root mean square of the conditioned signal and a third channel was used to record a verification signal specifying the position of the bubble nose. When the bubble remained stationary, a switch was depressed which caused the pen of the third channel to deflect. The verification signal was maintained as long as the bubble remained fixed in location and was discontinued when the bubble moved an axial distance greater than 0·5 mm. The bubble position was then noted on the strip-chart paper. This process was repeated for various locations of the measuring point and for a range of relative bubble positions. A composite picture of the velocity field inside the breakdown envelope was produced in this way.

In the discussions that follow, axial locations are given relative to the apparent nose of the bubble, negative values indicating upstream positions and positive values downstream positions. For reference, it should be noted that for these flow conditions the mean location of the bubble nose was 3 mm upstream of the beginning of the tube divergence, and the bubble length was 15·5 mm. In those cases where the radius has been non-dimensionalized, r_i is the tube radius at the axial location where the measurements were made.

5. Results: mean velocity

The three profiles of axial velocity shown in figure 3(*a*) were measured at three axial locations well upstream of the breakdown; all were characterized by features evident in the inlet flow profiles presented in FL. A region of high velocity occurred near the tube centre-line, followed by a region in which the axial velocity was nearly constant with r with a slight increase in velocity just inside the wall boundary layer. At $-30{\cdot}6$ mm, which we take as our 'inlet' station, and at $-22{\cdot}6$ mm, velocity readings were unaffected by the slight changes in bubble position, while at $-14{\cdot}6$ mm slight changes in velocity were noticeable near $r = 0$ as the bubble wandered axially. The profiles varied little with axial distance until the presence of the bubble affected the flow.

For flows in the present apparatus at higher Reynolds number, Faler & Leibovich

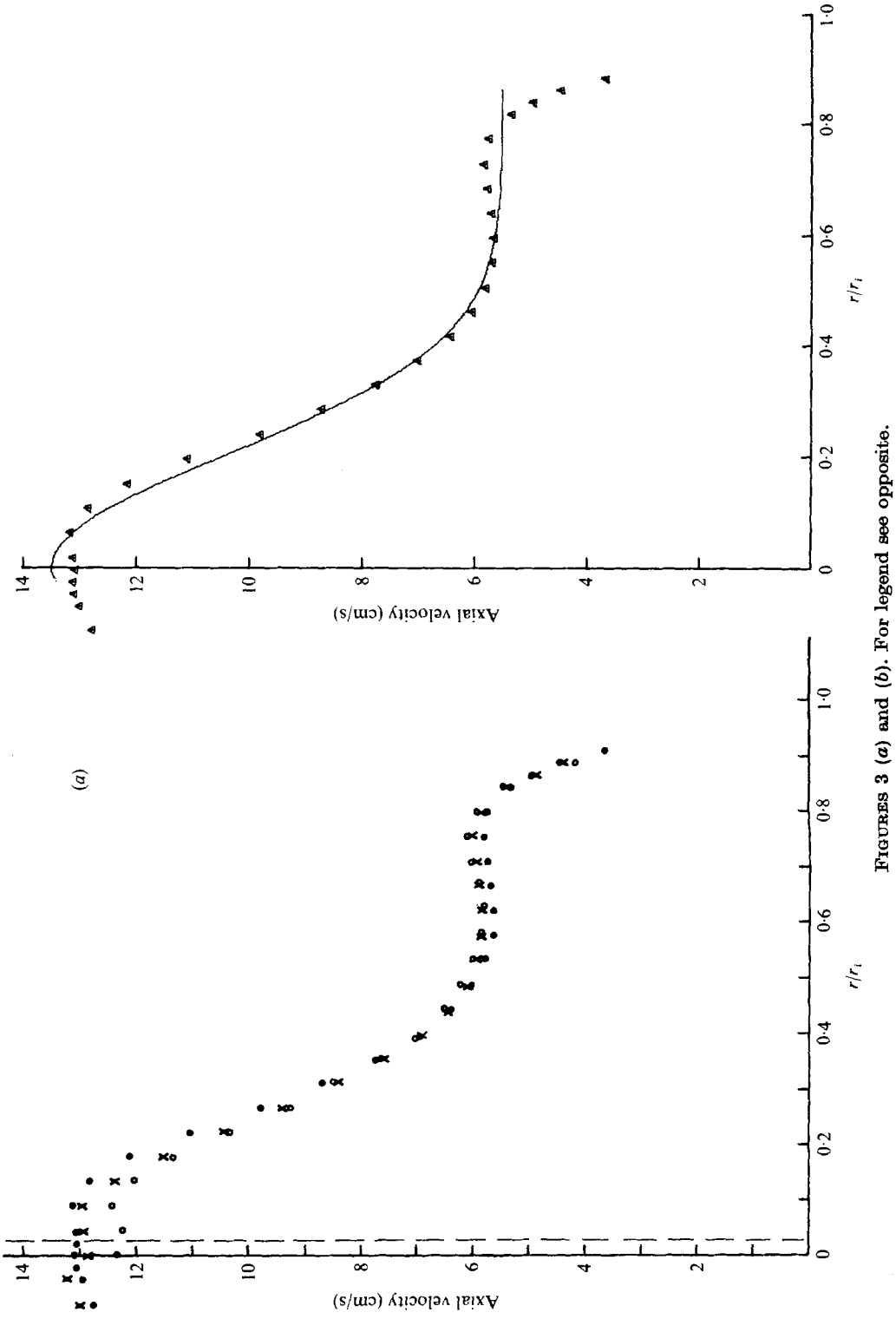

FIGURES 3 (*a*) and (*b*). For legend see opposite.

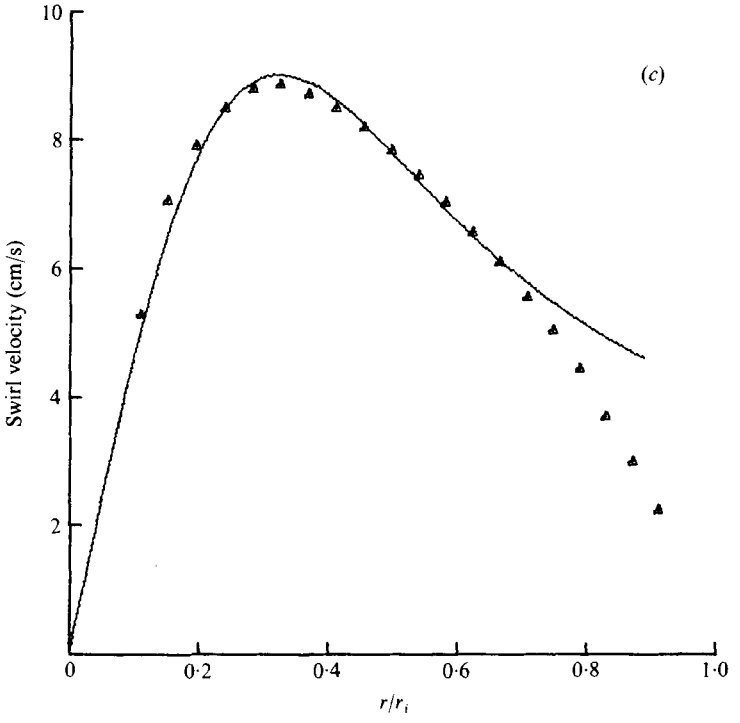

FIGURE 3. (*a*) Axial velocity *vs.* non-dimensional radius; $Re = 2560$, $\Omega = 1{\cdot}777$. Axial distance (distance upstream of bubble nose): ●, $-30{\cdot}6$ mm; ×, $-22{\cdot}6$ mm; ○, $-14{\cdot}6$ mm. The dashed vertical line gives the location of the true axis of symmetry as discussed in the text. (*b*) Profile of the axial velocity component for conditions of (*a*). The solid line indicates the least-squares best fit to (1*a*). Symbols indicate experimental data. (*c*) Profile of the swirl velocity component for the inlet conditions leading to (*a*). The solid line is the least-squares best fit to (1*b*). Symbols indicate experimental data.

(1977) reported that the inlet axial and swirl velocity components outside the boundary layer on the tube wall are well fitted by

$$W(r) = W_1 + W_2 \exp(-\alpha r^2/r_t^2), \tag{1a}$$

$$V(r) = K(r/r_t)^{-1}[1 - \exp(-\alpha r^2/r_t^2)], \tag{1b}$$

where r_t is the tube radius at the inlet station. After correction for an error in locating the tube centre-line (discussed below), the present inlet data ($-30{\cdot}6$ mm) may also be fitted with acceptable accuracy by these formulae with $\alpha = 11{\cdot}84$, $W_1 = 5{\cdot}53$ cm/s, $W_2 = 7{\cdot}95$ cm/s and $K = 4{\cdot}1$ cm/s, as shown in figures 3(*b*) and (*c*). As FL pointed out, the method of generating the swirl as a radial inflow of a nearly irrotational swirling flow favours the production of the Burgers (1948) vortex (1*b*). This inflow is then redirected to produce an essentially cylindrical flow at the inlet station. The magnitude of α, and hence the size of the vortex core, is determined by the thickness of the boundary layer shed from the centre-body, and is expected to increase in proportion to Re. Studies by Garg & Leibovich (1978) in this apparatus at Reynolds numbers up to 21 000 show that (1) continues to fit the data, and that α is an approximately linear function of Re. This suggests that the natural unit of length in the radial direction is $(\nu r_t/\overline{W})^{\frac{1}{2}}$, which characterizes the radius of the vortex core. To facilitate

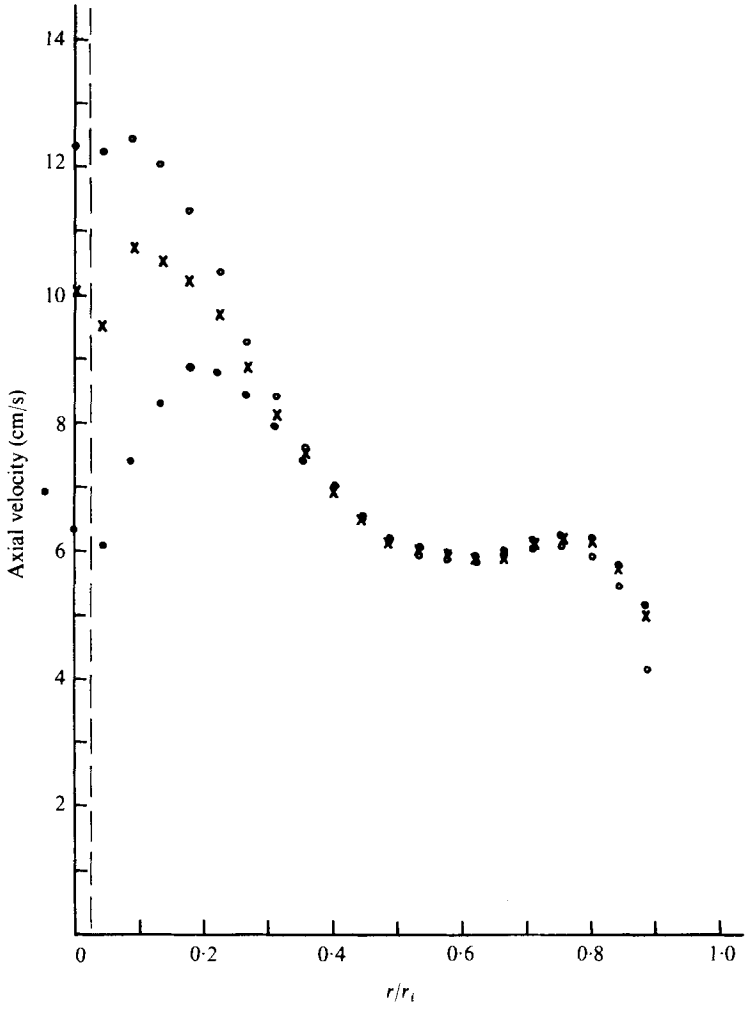

FIGURE 4. Axial velocity *vs.* non-dimensional radius; $Re = 2560$, $\Omega = 1{\cdot}777$. Axial location (distance upstream of bubble nose): ○, $-14{\cdot}6$ mm; ×, $-6{\cdot}6$ mm; ●, $-4{\cdot}0$ mm.

comparison with previous results, however, we have retained r_t as our reference dimension. After the vortex core has been formed, the flow may be reasonably approximated as inviscid at the Reynolds number considered here, except for the wall boundary layer. Inviscid total head considerations for a cylindrical flow then reveal that an axial velocity jet on the axis may be expected.

As may be seen in figures 4 and 5, the centre-line axial velocity decreased rapidly in the region extending from $-14{\cdot}6$ mm to the breakdown nose. This rapid deceleration reduced the centre-line velocity from its maximum value to zero in an axial distance of ~ 15 mm, or one bubble length, as shown in figure 6. The collapse of the high velocity jet near $r = 0$ led to a slight increase in velocity in the flat region of the profile ($r/r_i = 0{\cdot}5$–$0{\cdot}7$) and a more noticeable increase closer to the tube wall, indicating the thinning of the boundary layer appropriate in a locally favourable pressure gradient.

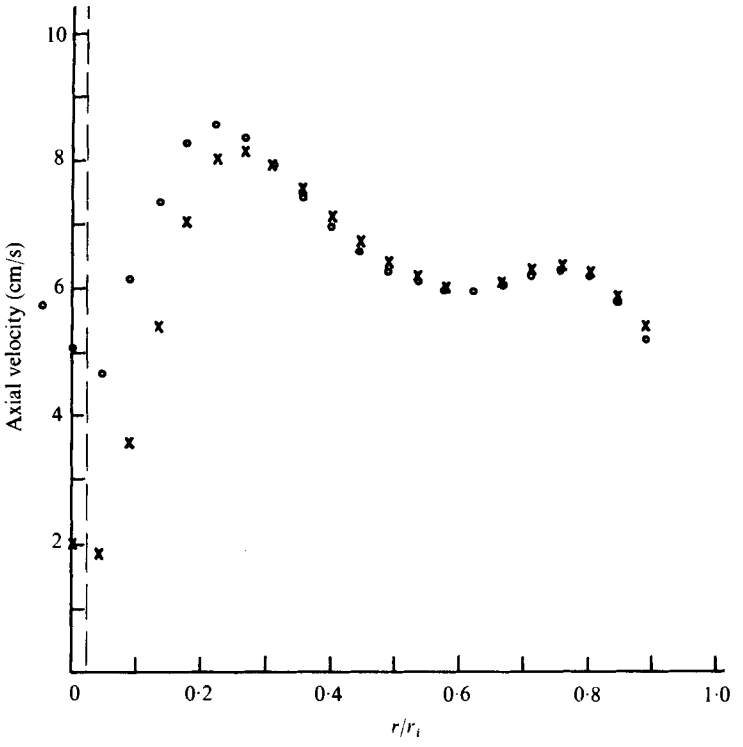

FIGURE 5. Axial velocity *vs.* non-dimensional radius; $Re = 2560$, $\Omega = 1{\cdot}777$. Axial distance (distance upstream of bubble nose): ○, −3·0 mm; ×, −1·0 mm.

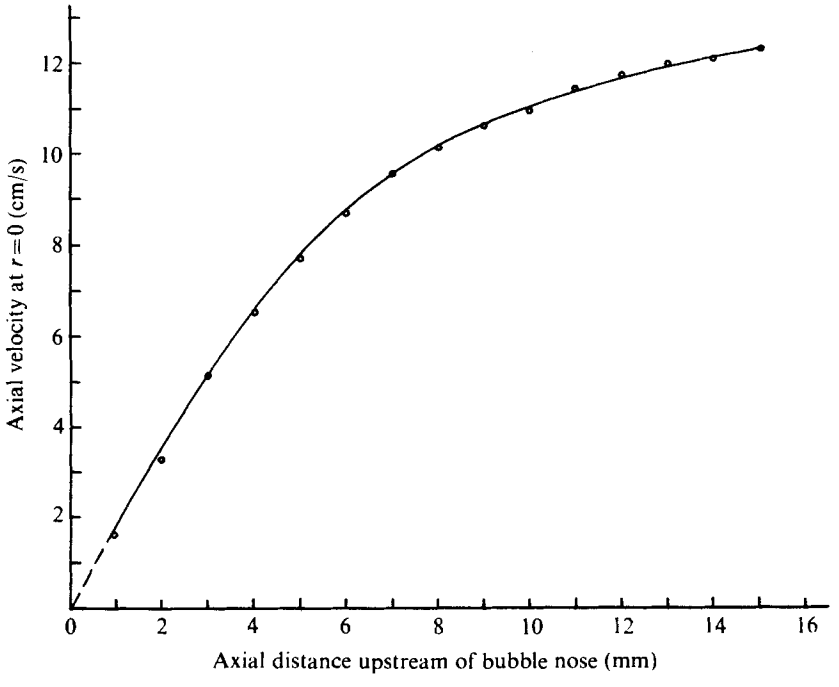

FIGURE 6. Decay of centre-line axial velocity as the breakdown is approached.

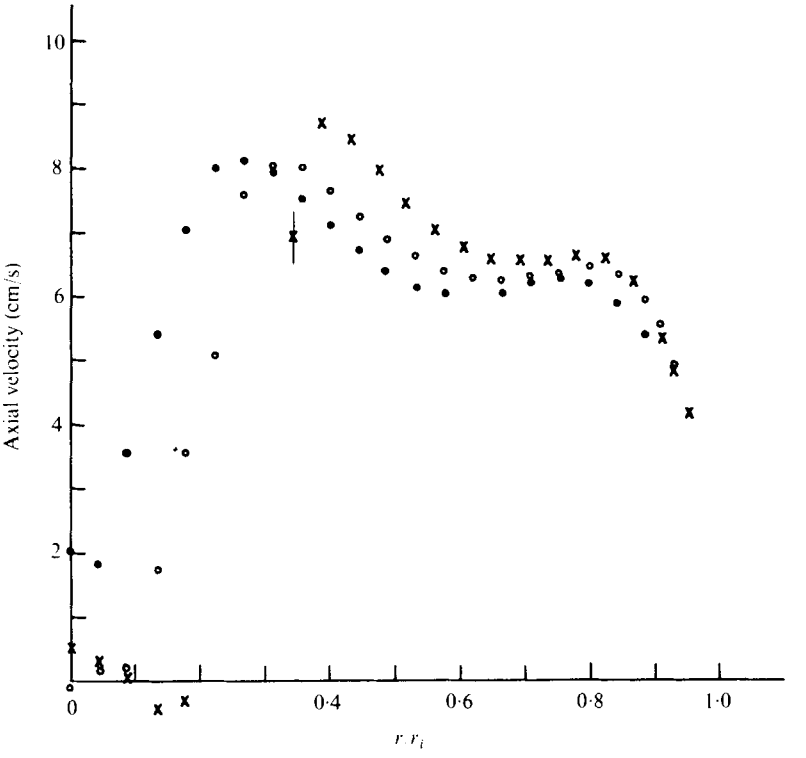

FIGURE 7. Axial velocity *vs.* non-dimensional radius; $Re = 2560$, $\Omega = 1{\cdot}777$. Axial location (distance upstream (−) and downstream (+) of bubble nose): ●, −1 mm; ○, +1 mm; ×, +8 mm.

All profiles shown in figures 3–5 were measured using the same initial alignment to determine $r = 0$. The profile shapes indicate that the centre-line was actually located at $r/r_i \approx 0{\cdot}028$, as marked by the dashed line in figures 3(*a*), 4 and 5. Since the nominal centre-line is located visually by positioning the laser beam probe volume on the axial dye filament, a maximum potential mislocation of this amount is possible.

The −1 mm profile is repeated in figure 7 as a reference for comparison with the profiles measured at stations +1 mm and +8 mm downstream of the bubble nose. Figure 8 gives the profiles +10, +15 and +24 mm downstream of the nose. Notice that the outward displacement of the fluid caused by the presence of the bubble resulted in a substantial increase in velocity for r/r_i greater than about 0·35. The bubble diameter was a maximum at about +10 mm and thus the area of the annulus defined by the tube wall and bubble envelope was a minimum at this location. This is reflected by the relatively high velocities in the +10 mm profile between $r/r_i = 0{\cdot}4$ and $r/r_i = 0{\cdot}7$. Large radial gradients occur near the bubble envelope $r/r_i \approx 0{\cdot}3$, as shown in the +8, +10 and +15 mm profiles, and low and reversed axial velocities occur in the interior of the RZ. The +24 mm station is in the near wake of the breakdown. For reference, the (mean) rear stagnation point of the RZ was at +16 mm, and the kink of a secondary spiral breakdown that inevitably occurred downstream of a breakdown bubble (as discussed by FL) was located at approximately +30 mm. A wake-like momentum defect downstream of the bubble is apparent, and this defect

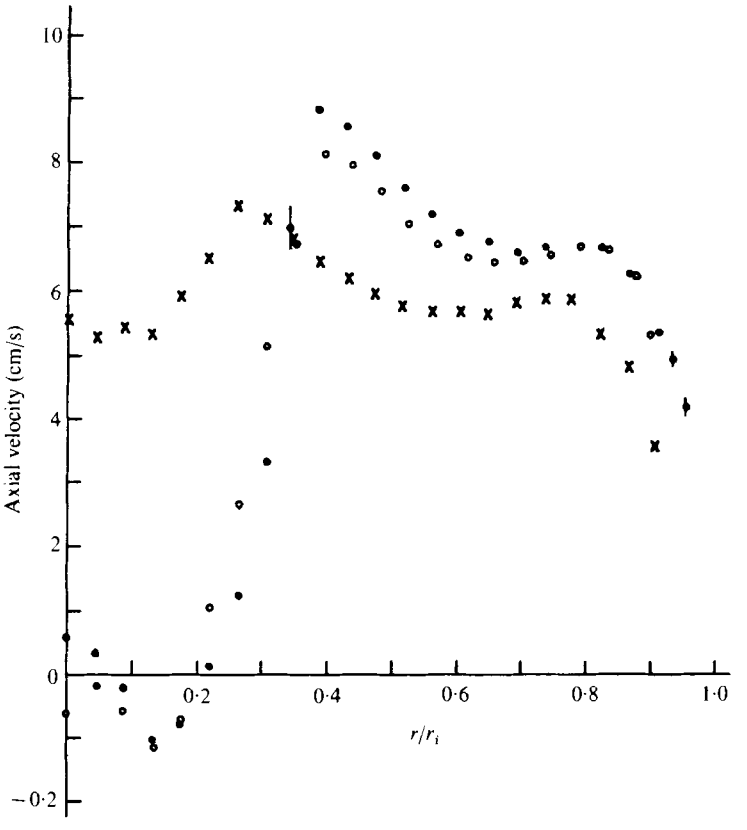

FIGURE 8. Axial velocity *vs.* non-dimensional radius; $Re = 2560$, $\Omega = 1{\cdot}777$. Axial location (distance downstream of bubble nose): ●, + 10 mm; ○, + 15 mm; ×, + 24 mm.

persists for all stations (not presented in this paper) downstream. In the far wake (achieved a few vortex core radii downstream of the rear of the RZ), experiments by Garg & Leibovich (1978) show that a more conventional, smooth wake profile is established and that the flows subsequently change slowly with axial distance. A comparison between the + 15 mm and the + 24 mm profile shows a substantial increase in the thickness of the wall boundary layer in the latter profile, presumably due to the adverse wall pressure gradient in this region.

A global check on these measurements was done by computing the volume flow rate by numerical integration of several profiles. Agreement between volume flow rates at different stations was good. For example, when the centre-line adjustment mentioned previously was made for the upstream profiles, less than a 1 % difference existed between the volume flow rate calculated at − 30·6 mm and that calculated at + 24 mm.

The results of the axial velocity measurements inside the bubble revealed an entirely unexpected structure. As shown in figure 9, the data for the time-averaged velocity indicate that four stagnation points existed (marked by the letter S in the figure) along the axis. Axial positions are referred to the apparent nose of the bubble as in the other figures; the bubble envelope superimposed on the figure was determined from photographs and streamline calculations based on mean velocity data.

The region of reversed velocity at $r = 0$ near the nose (0·5–2·5 mm) was characterized

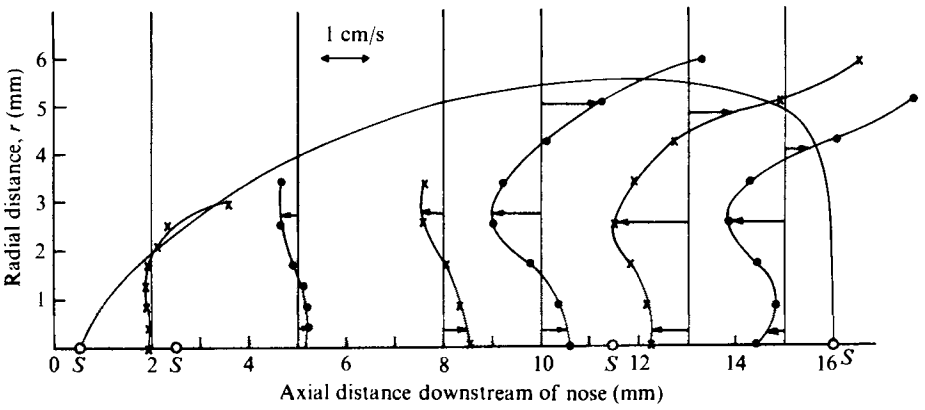

FIGURE 9. Mean (time-averaged) axial velocity profiles inside the bubble; $Re = 2560$, $\Omega = 1{\cdot}777$. The S's denote the four stagnation points.

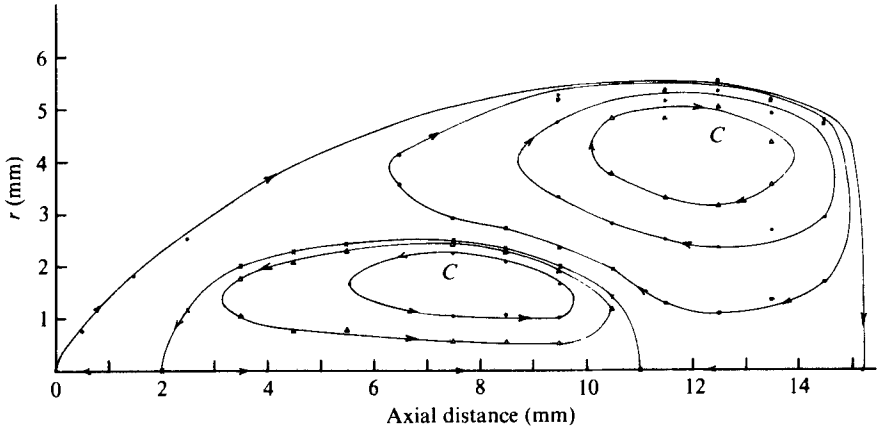

FIGURE 10. The mean streamline pattern inside the breakdown. The C's denote the centres of the recirculation cells.

by very small absolute values of the mean velocity and very weak fluctuations. The velocity on the axis was streamwise again from the second stagnation point at + 2·5 mm to the third one at + 11·5. Both the mean velocities and the fluctuation amplitudes were higher in this region than in the nose region. The downstream section of the bubble, from + 11·5 mm to the rear stagnation point at + 16·0 mm, features both the largest absolute values of reversed velocity and the highest amplitude fluctuations. The highest velocities inside the bubble were positive (streamwise), occurred near the envelope, and were about 15 % of the maximum centre-line velocity measured upstream of the breakdown. The reversed mean velocities were largest at $r \approx 2{\cdot}5$ mm and 11–13 mm downstream of the nose and were about 12 % of the maximum centre-line velocity upstream of breakdown. The reversed velocities decreased in absolute value upstream of + 11 mm as the recirculated fluid moved upstream and towards the bubble envelope.

The mean stream surfaces in figure 10, constructed by numerically integrating time-averaged axial velocity data, are of help in visualizing flow patterns in the recirculation zone. Mean velocity data are of limited physical value when large amplitude

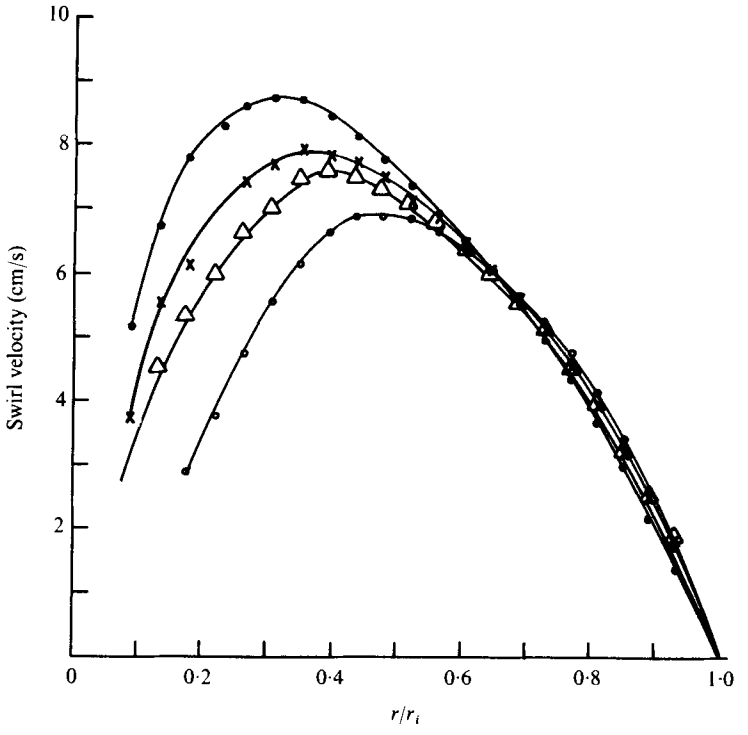

FIGURE 12. Swirl velocity *vs.* non-dimensional radius; $Re = 2560$, $\Omega = 1{\cdot}777$. Axial location (distance upstream of bubble nose): ●, −22·6 mm; ×, −6·0 mm; ○, 0 mm; △, −3·0 mm.

fluctuations are present. In the present case, however, fluctuations larger than mean values are confined to a specific subregion in the rear third of the RZ. Consequently, the mean velocity data, and mean streamlines derived from them, provide useful information, including an estimate of instantaneous flow patterns, for a significant fraction of the bubble interior.

The bubble envelope in figure 10 (the outer mean dividing streamline) was determined from the mean velocity data and several enlarged photographs. Axial distance in this figure is referred to the front stagnation point. The most interesting feature of the mean streamline pattern is a two-celled structure in the bubble interior. The larger, outer cell recirculated about 1 % of the total volume rate of flow through the tube. Only a small fraction of this recirculated fluid reached the upstream section of the bubble, and most of the recirculating fluid in this outer cell was confined to the rear half of the bubble. The inner cell was significantly weaker than the outer one and recirculated only 3·7 % of the mean amount of fluid carried by the outer cell. The stagnation point marking the downstream end of the inner cell separated a region of relatively weak fluctuations inside the inner cell from a region of strong fluctuations in the downstream section of the bubble. The directions of the instantaneous, as well as mean, axial velocities on the axis between each pair of mean stagnation points are as shown in figure 10.

The existence of an inner cell may be detected visually, although without the construction from velocity data one would have no basis on which to interpret the visual evidence as another cell of extremely slowly moving fluid. The photographs

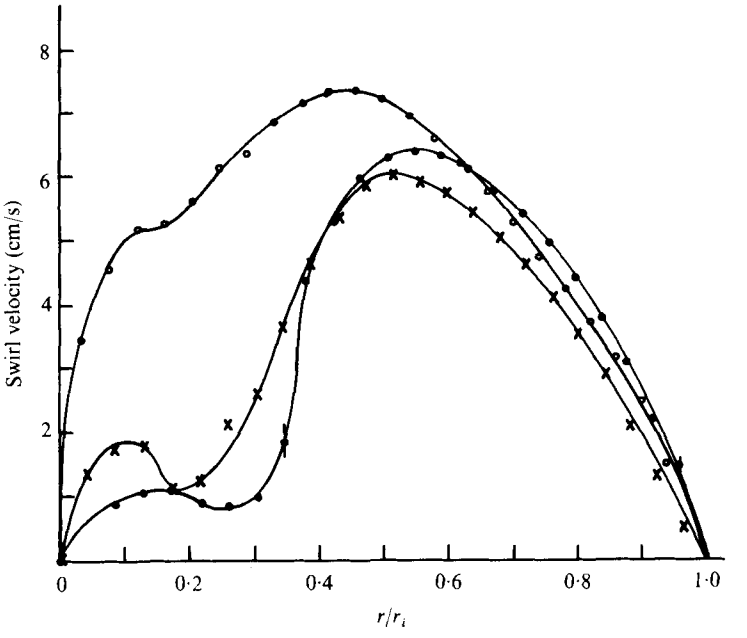

FIGURE 13. Swirl velocity *vs.* non-dimensional radius for $Re = 2560$, $\Omega = 1{\cdot}777$. Axial location (distance downstream of bubble nose): ●, +8·0 mm; ×, +15·0 mm; ○, +24·0 mm.

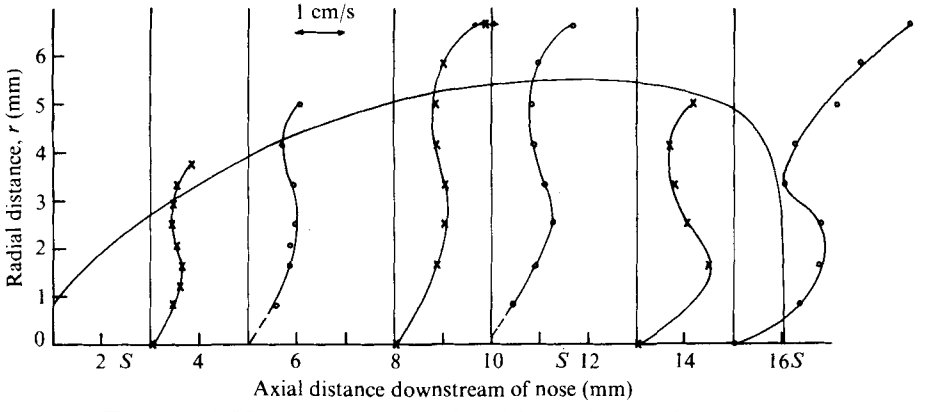

FIGURE 14. Mean (time-averaged) swirl velocity profiles inside the bubble; $Re = 2560$, $\Omega = 1{\cdot}777$.

shown in figure 11 (plate 1) were taken sequentially over a period of about 12 s after interrupting the flow of dye. The nearly quiescent inner core can be seen clearly, being indicated by the dark streak located on the bubble centre-line and extending from the nose region to a point about two-thirds of a bubble length downstream of the nose. The existence of this inner core and its streamwise axial velocity on the tube centre-line are in agreement with the behaviour of the 'screw worm' filament described by Faler (1976) and by FL.

The swirl velocity profiles at the bubble nose and at three upstream stations are shown in figure 12. As shown, the radial position at which the swirl velocity was a maximum moved outwards significantly as the bubble was approached.

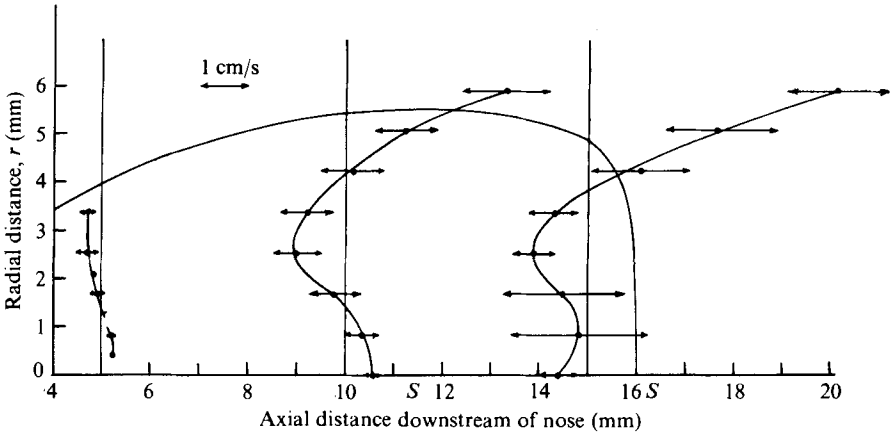

FIGURE 15. The amplitude of the axial velocity fluctuations, represented by the horizontal bars, inside the breakdown; $Re = 2560$, $\Omega = 1{\cdot}777$.

Three swirl velocity profiles measured downstream of the bubble nose are shown in figure 13. The sharp increase in angular velocity near the centre-line at +24 mm, in the near-wake region, resulted from the convergence of the flow downstream of the breakdown. The prominent dip in the mean swirl velocity near the bubble envelope ($r/r_i \sim 0{\cdot}2$) shown in the +8 and +10 mm profiles is still evident at the +24 mm location. The decrease in swirl velocity at, or just inside, the bubble envelope for each axial station, as seen in figure 14, is the most striking feature of the mean swirl velocity profiles measured inside the breakdown. For axial locations between 0 and +10 mm, the dip is relatively small in magnitude and the radial position at which the swirl was locally a minimum correlates well with the radial location of the breakdown envelope. The dip is significantly larger in magnitude in the downstream portion of the bubble and was located well inside the mean dividing streamline. This minimum mean swirl velocity near the RZ envelope can be explained as follows. Visual observations (e.g. Sarpkaya 1971*a*; FL) show that fluid is exchanged between the RZ and the exterior flow by a periodic emptying and filling process at the back end of the bubble. Fluid particles close to the mean bubble envelope travel on trajectories originating near the tube axis, and therefore carry low angular momenta. Angular momentum is essentially conserved by fluid particles as they are displaced outwards. On the other hand, fluid particles passing points inside the RZ further away from the bubble envelope follow trajectories originating (far upstream) at positions further away from the axis, and therefore carry angular momenta larger than those near the RZ envelope. Consequently, the RZ envelope is a surface on which angular momentum attains a local minimum.

6. Results: velocity fluctuations

The discussion of the flow inside the breakdown has centred on time-averaged velocities. The dominant feature of flow inside the bubble and in the wake region, however, was a strong temporal oscillation. These oscillations are represented graphically in figures 15–17 by the bars superimposed on the mean velocity profiles measured inside the bubble (figures 15 and 16) and in the wake region (figure 17). The length

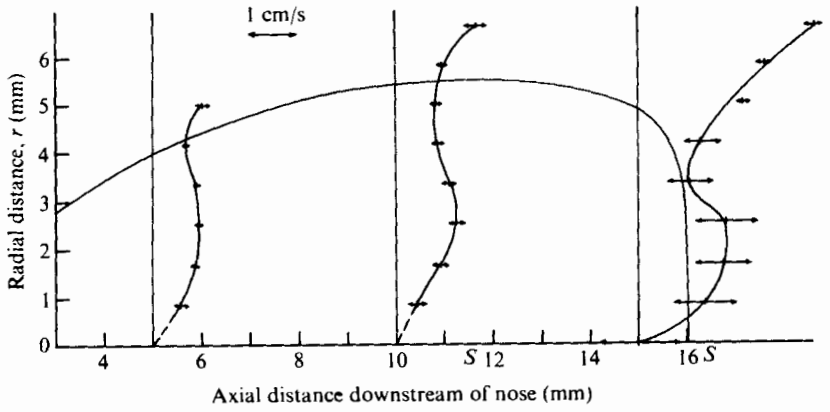

FIGURE 16. The amplitude of the swirl velocity fluctuations, represented by the horizontal bars, inside the breakdown; $Re = 2560$, $\Omega = 1{\cdot}777$.

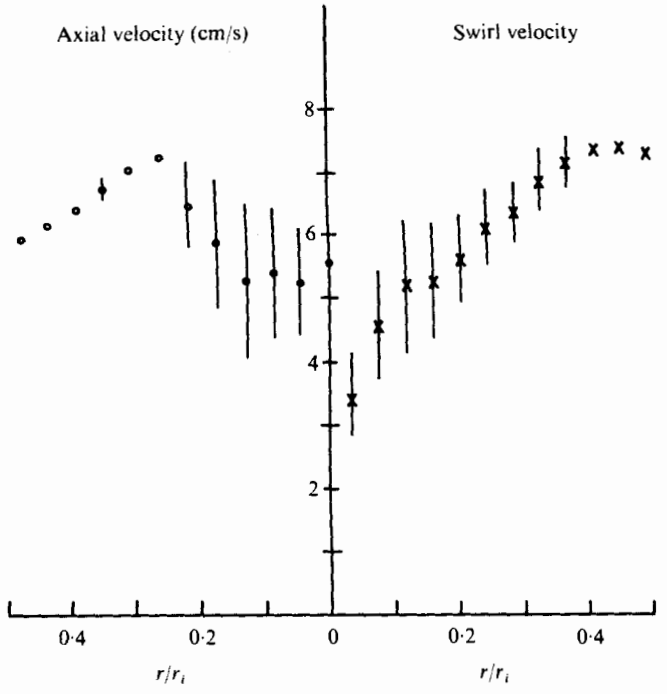

FIGURE 17. The vertical bars represent the amplitude of the axial and swirl velocity fluctuations in the wake of the breakdown; $Re = 2560$, $\Omega = 1{\cdot}777$, axial location $= +24$ mm.

of the bars represents the average peak-to-peak amplitude of the velocity fluctuations. In the cases represented in figures 15 and 17 the average amplitudes were estimated from the strip-chart records. Peak-to-peak amplitudes in figure 16 were estimated by multiplying the root mean square of the time-varying velocity (recorded on a separate channel) by $\sqrt{2}$, i.e. by assuming a sinusoidally varying velocity. It should be pointed out that the swirl velocity fluctuation amplitude at $r = 0$ may have a contribution from radial velocity fluctuations since very near the tube centre-line these components are not resolved by the laser-Doppler anemometer.

The amplitude of the temporal fluctuations was greatest at a location slightly off the axis in the rear portion of the bubble. In this region, the time-varying velocity was remarkably periodic and fluctuations resulted in a continual exchange of fluid across the mean dividing streamline. The temporal variations were weakest in the nose region of the breakdown and inside the inner cell as discussed previously. The change in the fluctuation amplitude was especially noticeable when measurements were made close to the centre-line near the stagnation point marking the downstream end of the inner cell. When the measuring volume was inside the inner cell the strip-chart trace showed relatively small fluctuations, and only small changes in fluctuation amplitude resulted as the bubble drifted axially as long as the probe volume remained inside the inner cell. However, when the bubble moved upstream far enough for the probe volume to cross the inner cell boundary, the fluctuation amplitude increased abruptly and the mean axial velocity became negative. The strong fluctuations in velocity resulting in the simultaneous emptying and filling of the bubble did not decay smoothly with increasing distance upstream of the rear stagnation point; instead, the amplitude was relatively constant in the rear portion and decreased rapidly near the stagnation point at the downstream end of the inner cell.

Velocity fluctuations varied in nature from region to region within the bubble. For example, fluctuations in the nose region were small and random in nature, with no apparent dominant frequency. Fluctuations were generally noticeable near the bubble envelope, but the traces were characterized by random 'spikes' superimposed on a signal with rather small fluctuations; fluctuations at $r = 0$ (especially in axial velocity) were also less regular. In other regions of the bubble (especially in the downstream half) and in the wake regions, fluctuations were highly periodic.

In regions of regular velocity fluctuations the dominant frequency could be estimated by counting the numbers of cycles contained in a given length of record. To determine the dominant frequency characteristics more precisely, velocity spectra were calculated. The analog voltage–time trace was sampled at a rate of 0·04 s and each set of data, representing a time series of a velocity component at a fixed position inside the bubble, was frequency analysed on a digital computer. Covariances and spectra were calculated using a Parzen lag window as described in Jenkins & Watts (1968, chap. 7). Data were digitized manually, an extremely tedious task, and therefore only a limited number of locations were selected for analysis.

The spectra shown in figure 18 were computed from the axial velocity data on a plane 12 mm downstream from the front stagnation point; the bandwidth in each case is 1·33 Hz. All spectra shown have peaks at 2·1 Hz, indicating the presence of periodic fluctuations at this frequency. In addition, the spectra show, to varying degrees, a peak at the first harmonic, 4·2 Hz. The spectrum for $r = 2{\cdot}54$ mm indicates that the fundamental and first harmonic contained comparable amounts of energy. The spectrum on the centre-line at this axial station (not shown) displays significant peaks at slightly higher frequencies (2·7, 4·6 Hz). The spectrum for the velocity near the dividing streamline ($r = 5{\cdot}07$ mm) at this axial station is characterized by the lack of a dominant peak and indicates less ordered fluctuations.

The dominant frequency varied only slightly from position to position inside the bubble, as long as the mean axial location of the breakdown was constant. This frequency changed more noticeably, however, over a range of 1·7–2·1 Hz, when the mean bubble position changed from day to day; the higher frequency corresponded

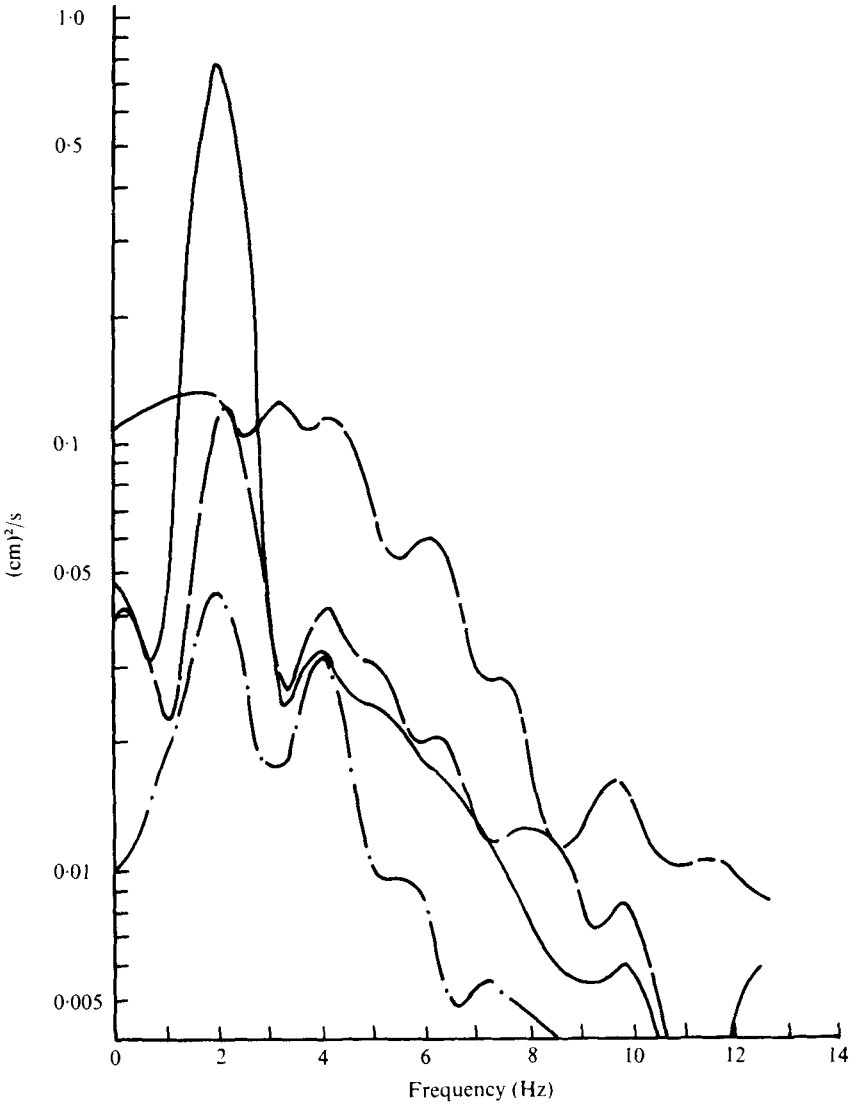

FIGURE 18. Power spectra of the axial velocity component inside the breakdown envelope at a plane 12 mm from the front stagnation point. ——, radial position $r = 1{\cdot}69$ mm; —·—, $r = 2{\cdot}54$ mm; — — —, $r = 3{\cdot}38$ mm; — — —, $r = 5{\cdot}07$ mm. The bandwidth in each case is 1·33 Hz.

to a location further upstream. The dominant frequency showed no correlation with the characteristic frequency obtained by dividing the average swirl velocity at the bubble envelope by the bubble circumference. There is excellent agreement, however, between this fundamental frequency and the angular frequency at which the rear portion of the single-tailed bubble rotated about the tube axis. It can be inferred, then, that the temporal periodicity and the azimuthal periodicity are related to each other, and associated with the simultaneous emptying and filling at the regularly rotating tail section of the bubble. It is possible that the flow is steady but asymmetric in a rotating reference frame. We are unable to settle this question, but observations of

the related 'flattened bubble' (type 4) breakdowns occurring earlier in the hierarchy of disturbance forms described by FL suggest that the present flow need not be steady in any reference frame.

7. Concluding remarks

The velocity profiles at all stations upstream of breakdown (figures 3, 4, 5, 12 and 13) as well as the time-averaged data in the breakdown wake (figures 8 and 14, data labelled +24 mm) have been analysed to determine whether they are subcritical or supercritical according to Benjamin's (1962) classification. All stations upstream of −3 mm were supercritical while the station at −3 mm and those further downstream were subcritical. Benjamin's theory and classification scheme contemplate a flow without axial variations, so that the application of his ideas to regions near the breakdown (−6 mm to +24 mm) is not strictly appropriate. Nevertheless, it is interesting that the flow further upstream is supercritical while the flow downstream is subcritical, as Benjamin's theory requires. The inlet flows (well upstream of breakdown) measured by FL were subjected to the same tests and all were found also to be supercritical. (Flows upstream of breakdown probably *must* be, upon reflexion, supercritical, so confirmation of this aspect of Benjamin's theory is expected in any event. This follows since, if the upstream flow were subcritical, long waves that by definition can propagate upstream would signal the presence of the breakdown, and upstream flow conditions would be disturbed.)

Leibovich (1978) points out that the stability results of Lessen, Singh & Paillet (1974) can be applied to the *inlet* profiles. When this is done, inlet profiles for which vortex breakdown occurs are found to be stable to all infinitesimal perturbations, both axisymmetric and otherwise.

The unexpected inner eddy of the two-celled internal structure revealed in figure 10 presumably is connected with the strong, very regular, azimuthally asymmetric fluctuations that occur inside the recirculation zone. This complexity is absent in solutions produced by numerical simulations based upon the axisymmetric, steady, Navier–Stokes equations. (See Kopecky & Torrance 1973; Grabowski & Berger 1976.) It would appear that no numerical simulation can be expected to produce a proper qualitative solution for the interior of the recirculation zone unless it is based upon the full (i.e. time-dependent and completely three-dimensional) Navier–Stokes equations.

It also seems clear, from the remarks on stability, that vortex breakdown cannot be explained as an ordinary hydrodynamic instability to non-axisymmetric perturbations, as proposed originally by Ludwieg (1962). Nevertheless, the appearance of azimuthal asymmetries in a flow with boundary conditions that are (experimentally) quite axially symmetric, and the important effects these asymmetrical motions have in the breakdown region show that instability is indeed manifest in these flows, and the role and origin of azimuthal asymmetries is a key open question.

We wish to thank Mr Amrish Garg for his assistance. This work was sponsored by NASA Grants NGL-33-010-042 and NSG 3019, technically monitored by the Lewis Research Centre.

REFERENCES

BENJAMIN, T. B. 1962 Theory of the vortex breakdown phenomenon. *J. Fluid Mech.* **14**, 593.

BENJAMIN, T. B. 1967 Some developments in the theory of vortex breakdown. *J. Fluid Mech.* **28**, 65.

BOSSEL, H. H. 1969 Vortex breakdown flow field. *Phys. Fluids* **12**, 498.

BURGERS, J. M. 1948 A mathematical model illustrating the theory of turbulence. In *Advances in Applied Mechanics*, vol. 1, p. 198. Academic Press.

CASSIDY, J. J. 1969 Experimental study and analysis of draft-tube surging. *U.S. Dept. Interior, Bur. Reclamation* REC-OCE-69-5, *Rep.* HYD-591.

ELLE, B. J. 1960 On the breakdown at high incidences of the leading edge vortices on delta wings. *J. Roy. Aero. Soc.* **64**, 491.

FALER, J. H. 1976 Some experiments in swirling flows: detailed velocity measurements of a vortex breakdown using a laser Doppler anemometer. Ph.D. dissertation, Cornell University. (Available as *N.A.S.A. Contractor Rep.* no. 135115.)

FALER, J. H. & LEIBOVICH, S. 1977 Disrupted states of vortex flow and vortex breakdown. *Phys. Fluids* **20**, 1385.

GARG, A. & LEIBOVICH, S. 1978 Experiments on oscillations in vortex breakdown flows. In preparation.

GARTSHORE, I. S. 1962 Recent work in swirling incompressible flow. *Nat. Res. Counc. Can. Aero. Rep.* LR-343.

GRABOWSKI, W. J. & BERGER, S. A. 1976 Solutions of the Navier–Stokes equations for vortex breakdown. *J. Fluid Mech.* **75**, 525.

HALL, M. G. 1967 A new approach to vortex breakdown. *Proc. Heat Transfer Fluid Mech. Inst.* pp. 319–340. Stanford University Press.

HALL, M. G. 1972 Vortex breakdown. *Ann. Rev. Fluid Mech.* **4**, 195.

HARVEY, J. K. 1962 Some observations of the vortex breakdown phenomenon. *J. Fluid Mech.* **14**, 585.

HUMMEL, D. 1965 Untersuchungen über das Aufplatzen der Wirbel an schlanken Deltaflügeln. *Z. Flugwiss.* **13**, 158.

JENKINS, G. M. & WATTS, D. G. 1968 *Spectral Analysis and its Applications*. Holden-Day.

KIRKPATRICK, D. L. I. 1964 Experimental investigation of the breakdown of a vortex in a tube. *Aero. Res. Counc. Current Paper* no. 821.

KOPECKY, R. M. & TORRANCE, K. E. 1973 Initiation and structure of axisymmetric eddies in a rotating stream. *Computers & Fluids* **1**, 289.

LAMBOURNE, N. C. & BRYER, D. W. 1961 The bursting of leading-edge vortices – some observations and discussion of the phenomenon. *Aero. Res. Counc. R. & M.* no. 3282.

LEIBOVICH, S. 1968 Axially-symmetric eddies embedded in a rotational stream. *J. Fluid Mech.* **32**, 529–548.

LEIBOVICH, S. 1970 Weakly nonlinear waves in rotating fluids. *J. Fluid Mech.* **42**, 803.

LEIBOVICH, S. 1978 The structure of vortex breakdown. *Ann. Rev. Fluid Mech.* **10** (to appear).

LEIBOVICH, S. & RANDALL, J. D. 1973 Amplification and decay of long nonlinear waves. *J. Fluid Mech.* **53**, 481.

LESSEN, M., SINGH, P. J. & PAILLET, F. 1974 The stability of a trailing line vortex. Part 1. Inviscid theory. *J. Fluid Mech.* **63**, 753–763.

LUDWIEG, H. 1961 Ergänzung zu der Arbeit: 'Stabilität der Stromung in einem zylindrischen Ringraum.' *Z. Flugwiss.* **9**, 359.

LUDWIEG, H. 1962 Zur Erklärung der Instabilität der über angestellten Deltaflugeln auftretenden freien Wirbelkerne. *Z. Flugwiss.* **10**, 242.

MAGER, A. 1972 Dissipation and breakdown of a wing-tip vortex. *J. Fluid Mech.* **55**, 609.

PECKHAM, D. H. & ATKINSON, S. A. 1957 Preliminary results of low speed wind tunnel tests on a Gothic wing of aspect ratio 1·0. *Aero. Res. Counc. Current Paper* no. 508.

RANDALL, J. D. & LEIBOVICH, S. 1973 The critical state: a trapped wave model of vortex breakdown. *J. Fluid Mech.* **58**, 495.

SARPKAYA, T. 1971*a* On stationary and travelling vortex breakdowns. *J. Fluid Mech.* **45**, 545.

SARPKAYA, T. 1971*b* Vortex breakdown in swirling conical flows. *A.I.A.A. J.* **9**, 1792.

SARPKAYA, T. 1974 Effect of the adverse pressure gradient on vortex breakdown. *A.I.A.A. J.* **12**, 602.

SQUIRE, H. B. 1962 Analysis of the vortex breakdown phenomenon. Part I. In *Mizellaneen du Angewandten Mechanik*, p. 360. Berlin: Akademie.

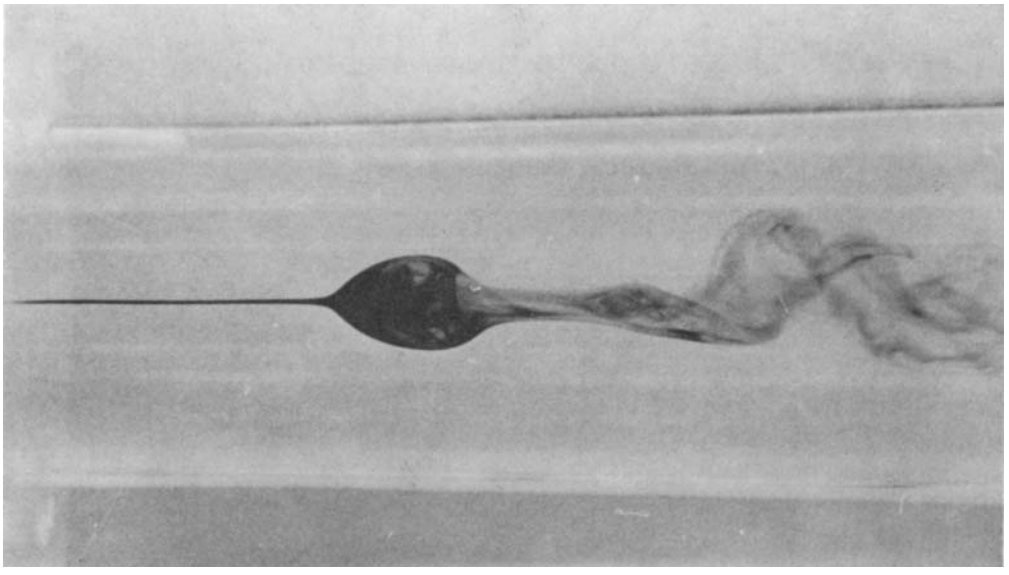

FIGURE 1. Photograph of the vortex breakdown investigated. This breakdown occurred at $Re = 2560$ and a swirl parameter $\Omega = 1{\cdot}777$ (cf. § 3). The mean position of the front stagnation point was 3 mm upstream of the beginning of the tube divergence. The interior of the breakdown is periodically emptied and filled at the rear end of the recirculation zone.

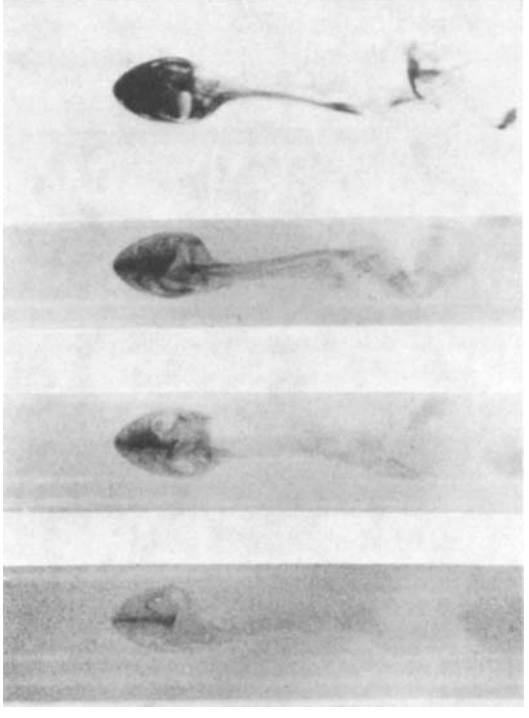

FIGURE 11. Sequence of photographs showing the inner recirculating cell. The first photograph was taken shortly after the upstream dye injection was interrupted. The darker region, which marks the inner core, remained visible for about 12 s.